J Appl Electrochem (2009) 39:523–528
DOI 10.1007/s10800-008-9713-1

ORIGINAL PAPER

# Possible proton conduction in $Ce_{0.9}Gd_{0.1}O_{2-\delta}$ nanoceramics

**Enrique Ruiz-Trejo · John A. Kilner**

Received: 3 September 2008 / Accepted: 29 October 2008 / Published online: 19 November 2008


**Abstract** Dense samples of $Ce_{0.9}Gd_{0.1}O_{2-\delta}$ with grain sizes in the range 91–252 nm were prepared and their electrical properties studied by impedance spectroscopy. It was found that the bulk conductivity is not affected by grain size or atmosphere and that small grain sizes lead to a larger total resistance of the material. The most striking result corresponds to a sample sintered in wet air that exhibited electrical characteristics that hint clearly at the presence of proton conduction at temperatures below 200 °C.

**Keywords** Nanoceramics · Gd-doped ceria · Proton conduction · Grain boundary

## 1 Introduction

Pure ceria and ceria-based materials present an interesting range of electrical transport properties. The doping of cerium oxide in the series $Ce_{1-x}Ln_xO_{2-x/2}$ (Ln = lanthanides$^{3+}$ or $Y^{3+}$, $x = 0.1, 0.2, 0.3$) produces the characteristic high oxygen-ion mobility [1] that makes it the ideal electrolyte for intermediate temperature Solid Oxide Fuel Cells (500–700 °C). However, this series can also exhibit electronic or mixed ionic-electronic conduction in reducing atmospheres [2–4]. It has also been reported that water can be incorporated into the lattice at high temperatures to produce proton conduction [5, 6]. Very recently, Kim et al. [7] have reported the possibility of proton conduction in nanoceramics of Sm-doped ceria by producing power with a simple concentration cell at room temperature.

It has also been shown that electronic conduction can occur in non-doped ceria when the grain size is below 100 nm [8–11]. The nature of the electrical conductivity in nanograin-sized heavily doped ceria is not yet thoroughly understood although great progress has been made with the space charge theory [9] in pure or slightly doped cerium oxide. There are recent claims that the ionic conductivity of $Ce_{0.8}Ln_{0.2}O_{2-d}$ (Ln = Sm, Y) increases with decreasing grain size at temperatures below 200 °C [12, 13] while for Sm-doped $CeO_2$ other authors find diminishing conductivity levels as the grain size decreases [14]. A clear dependence of dc conductivity with grain size for Y-doped $CeO_2$ has also been reported [15] while an enhancement in conductivity for Y and Gd doped $CeO_2$ [16, 17] in relatively mild reducing conditions using high purity nitrogen gas has been observed. There are also indications that a decreasing grain size induces an increasing electronic conductivity [18]. Yet, one of the most surprising reports is the aforementioned probable occurrence of proton conduction in nanoceramics of Sm-doped ceria [7].

In this work, a study of the electrical conductivity of materials with different grain sizes was undertaken. The effect of humidity in the electrical properties of the materials was investigated since it is known that water can readily interact with oxide surfaces. The obtained results hint at the possibility of proton conduction in this material.

## 2 Experimental

Samples of $Ce_{0.9}Gd_{0.1}O_{2-\delta}$ were prepared from commercial powders (Fuel Cell Materials, surface area 177.68 $m^2\ g^{-1}$).

E. Ruiz-Trejo (✉) · J. A. Kilner
Materials Department, Imperial College, London
SW7 2AZ, UK
e-mail: enrique.ruiz_trejo@servidor.unam.mx

E. Ruiz-Trejo
Facultad de Química, Departamento de Física y Química Teórica, Universidad Nacional Autónoma de México, Coyoacán 04510, Mexico, D.F., Mexico

The powders were first heated at 450 °C for 0.5 h in air and then cooled and pressed isostatically in a rubber mould at 300 MPa for 1 minute. The discs obtained were then heated at 600 °C/h up to the desired temperature (900–1200 °C). The dwelling time at each temperature was 6 min. These samples were used to study the effect of grain size in the transport properties.

An electron microscope (Gemini 1525 FEG-SEM) was used to study the microstructure of the samples in as-fractured surfaces. Since the samples are quite resistive at room temperature, gold coating was used. A rough estimation of the grain size was performed with the linear intercept method [19]. The density of the samples was measured with the Archimedes's method using deionised water as the immersion fluid.

The electrical conductivity of the samples from 350 to 100 °C was performed by impedance spectroscopy using a Solartron 1260 FRA in the frequency range between 1 Hz and 13 MHz. Silver paint was used as electrodes. This was applied at room temperature and then heated at 350 °C for 3 h before beginning the measurements. The impedance spectra were fitted with an equivalent circuit containing a resistance and a constant phase element (CPE) in parallel to model the bulk and a similar arrangement for the grain boundary. Both the bulk and the grain boundary equivalent circuits were in series with each other. The electrode was not modelled as this response was only seen at the highest temperatures but was not detected at lower temperatures. The capacitance of bulk and grain boundary was estimated from the CPE element according to reference [20].

To measure the effect of the water in the electrical conductivity of the nanoceramics a sample was prepared as indicated above but the sintering temperature was 1000 °C for 6 minutes in a current of synthetic air bubbled through water at room temperature ($pH_2O = 0.029$ atm). The impedance spectroscopy of this material was measured with a Dielectric Interface (1296 Solartron) coupled with a Solartron 1260 FRA. First, a set of impedance measurements was taken in zero grade air ($pH_2O < 0.003$ atm) and then a second set of measurement was performed in humidified air. All measurements began at 350 °C and then the temperature was decreased every 25 °C, with an equilibration time of 3 h at each temperature. In a different experiment with the same sample, the impedance of the sample at 200 °C was measured as a function of time at 4 different partial pressures of water.

## 3 Results and discussion

### 3.1 Microstructure

The samples displayed a density higher than 90% in all cases. Figure 1 presents the microstructure of samples prepared in atmospheric air and sintered at different temperatures. The samples are very dense with no visible pores or cracks. It is also observed that the average grain size increases with the temperature of sintering. At larger grain sizes, the mechanism of fracture seems to change. Figure 1a and b show that the fracture left the grains intact.

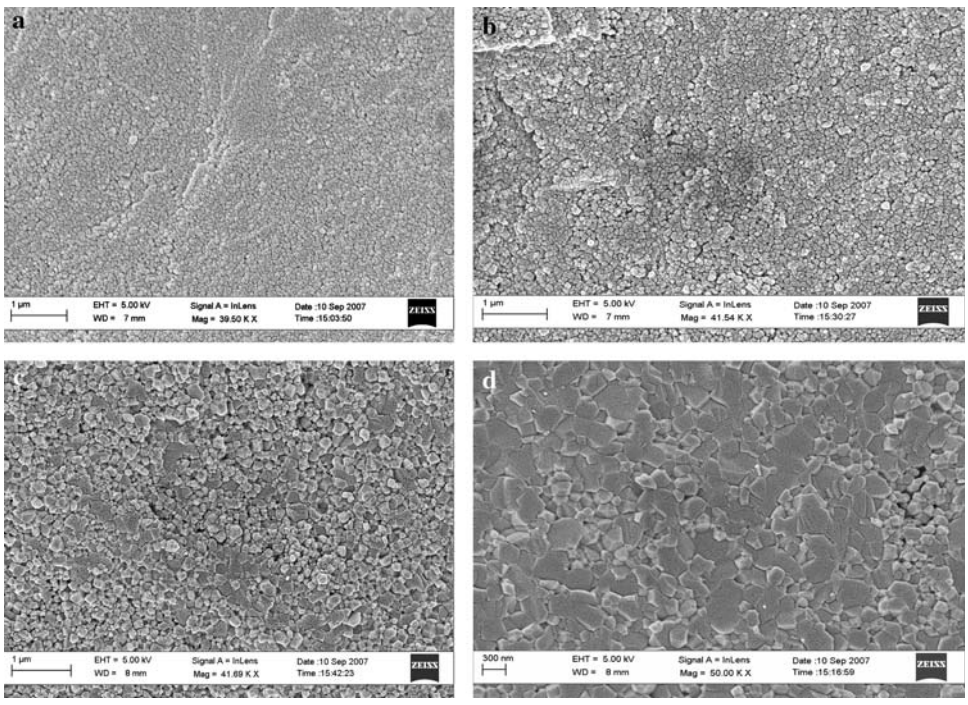


**Fig. 1** Microstructure of samples sintered at various temperatures. The grain sizes are also indicated. **a** 900 °C, 91 nm, **b** 1000 °C, 108 nm, **c** 1100 °C, 167 nm, **d** 1200 °C, 252 nm. All images correspond to fracture surfaces

On the other extreme, Fig. 1c and particularly Fig. 1d show that a great deal of fractures ran through the grains in a transgranular fracture mode. The preparation of these nanoceramics involved rapid heating of compact bodies of nanoparticles and this may produce mechanical stresses leading to fissures in some pellets. Nonetheless, it is important to point out that even though some of our samples were very brittle the samples used for impedance measurements did not show the presence of cracks.

### 3.2 Electrical characterisation

Figure 2 presents the impedance plots of the nanoceramics of $Ce_{0.9}Gd_{0.1}O_{2-\delta}$ shown in Fig. 1 measured in atmospheric air. Figure 2a shows that the bulk conductivity remains the same regardless of the grain size. An accurate determination of the bulk conductivity becomes increasingly difficult when the grain size is small as the semicircles start to overlap and consequently the fitting errors increase. As a smaller grain size leads to a large number of grain boundaries this component may dominate the total resistance of the samples as seen Fig. 2b for samples with the smallest grain size. The sample with 252 nm (sintered at 1200 °C) does not follow the trend since it displays a resistance slightly larger than that of 167 nm (sintered at 1100 °C). However, it must be remembered that these samples were measured in atmospheric air and may be reacting to the varying water content in the environment or it may be revealing a slightly different grain boundary structure or composition as a result of a different sintering temperature.

The bulk conductivity does not show a large variation with grain size as seen in Fig. 2a and displayed in Fig. 3 as an Arrhenius plot. The data of Steele for the bulk of $Ce_{0.9}Gd_{0.1}O_{1.95}$ [21] has been included as a reference. The activation energies display only marginal differences that may be the outcome of fitting errors only. In this grain size interval the bulk conductivity does not change.

Figure 4 displays the specific grain boundary conductivity $\sigma_{sgb}$ estimated according to [22] as

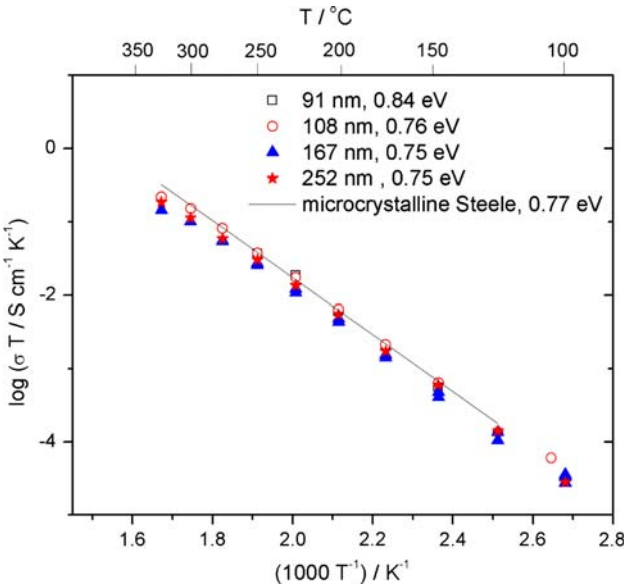


**Fig. 3** Bulk conductivity of samples with different grain size average. The label indicates the grain size and the activation energy found for each sample. The data of Steele [21] are taken as a reference for the microcrystalline material

$$\sigma_{sgb} = \frac{C_b \sigma_{gb}}{C_{gb}} \quad (1)$$

where $C_{gb}$ is the capacitance of the grain boundary, $C_b$ the capacitance of the bulk and $\sigma_{gb}$ is the conductivity measured from the impedance spectra. The specific grain boundary conductivity shows a variation with the grain size but unfortunately the limited number of values and their proximity does not allow us to establish a general trend. Furthermore, the results for small grain sizes hinder precise determination of $C_b$ necessary to use Eq. 1. It can be seen that the grain boundary activation energy is approximately the same, hinting at a similar type of conduction mechanism in the grain boundary in air. The value of 1 eV is typical for oxygen migration in $CeO_2$ and $ZrO_2$ based materials. The sample with 252 nm grain size was not

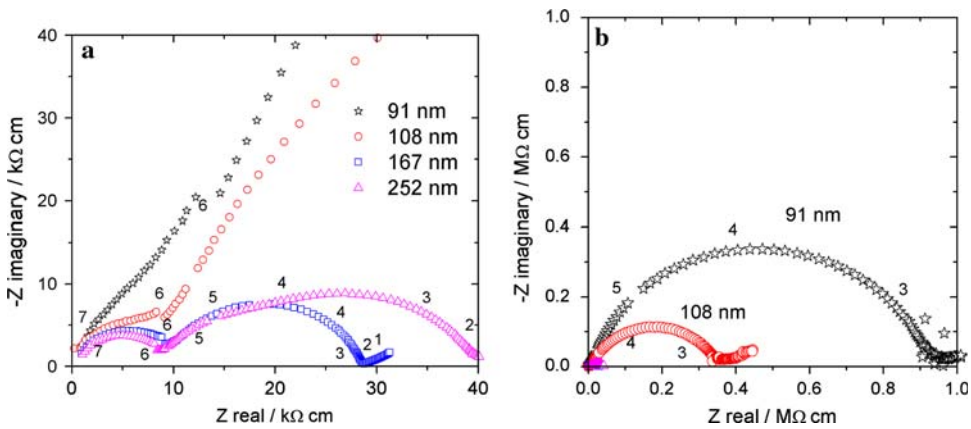


**Fig. 2** Impedance plot of nanoceramics of $Ce_{0.9}Gd_{0.1}O_{2-\delta}$ measured at 275 °C in air. The grain sizes are shown and the numbers indicate the logarithm of the frequency. Figure 2a shows the bulk region while Fig. 2b displays the whole range of impedance

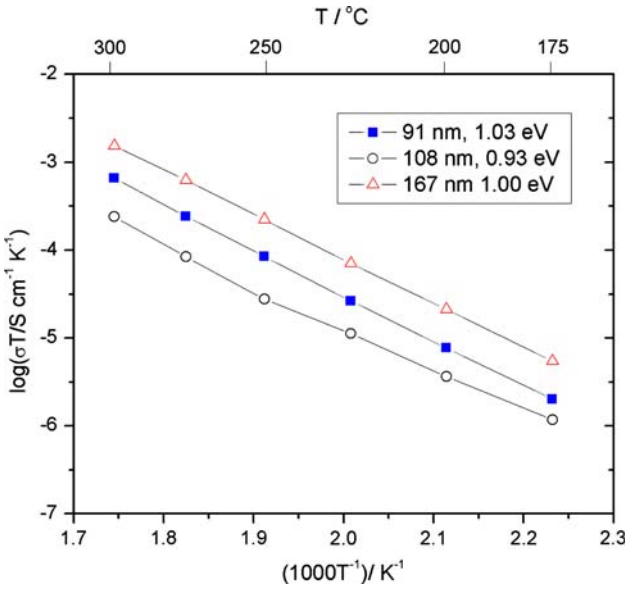


**Fig. 4** Arrhenius plots of the specific grain boundary conductivity for three different grain sizes. The activation energies are also indicated

included, since a unique value of the capacitance cannot be assigned to the grain boundary as can be seen from Fig. 2a.

### 3.3 Conductivity dependence with water vapour

A further sample was sintered at 1000 °C in wet air and then measured in air after manual application of silver electrodes at room temperature. Figure 5 shows the Arrhenius plot of the total conductivity of this sample; this clearly shows a difference between the same sample measured in dry ($pH_2O < 0.003$ atm) and wet ($pH_2O = 0.029$) air. The total

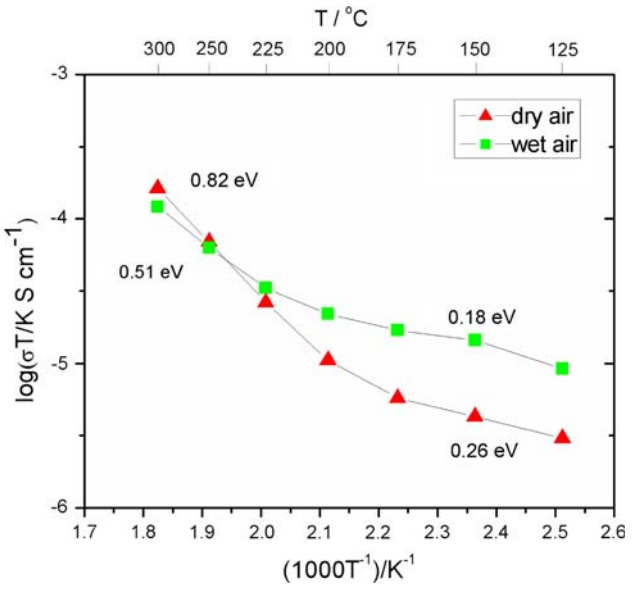


**Fig. 5** Arrhenius plot of the conductivity in wet (0.029 atm) and dry (<0.003 atm) air. The activation energies of the different regions are indicated

conductivity is slightly higher in wet atmospheres than in dry and this effect has an apparent temperature limit of 250 °C. Furthermore, there is a crossover of the conductivities at this point. Another clear change is the activation energy of the conductivity process. According to the experiments performed at 200 °C shown next, the samples were in equilibrium with the atmosphere.

To confirm that the sample conductivity depends upon the humidity of the atmosphere, the impedance of the sample was measured as a function of time after the changes in the water partial pressure at a fixed temperature of 200 °C. Figure 6a displays the bulk response in the impedance spectra of a sample measured in dry and wet air at 200 °C while Fig. 6b shows the complete spectra after the samples have reached equilibrium. Three features are clearly seen. Firstly, the bulk response remains the same regardless of the humidity level as expected for a purely oxygen ion conductor even though it has been suggested that water has a high solubility in ceria [5]. This suggestion is coupled with strong indications that this solubility is correlated to the basic nature of the rare earth dopants [6]. The second feature is a large response (tens of MΩ) that dominates the total resistance. It has been proposed that the grain boundaries may be very blocking due to the presence of a space charge layer [9] and this may be the origin of the large resistance. The third and most striking feature, as seen in Fig. 6b, is the clear difference of the total conductivity between wet and dry atmospheres. A capacitance of 18 pF was found for the high frequency semicircle, which corresponds to a bulk response. The other signal leads to a capacitance of 76 nF, a value usually associated to grain boundaries.

Figure 7 shows the total resistance as a function of time in wet and dry atmospheres. The total resistance was taken as the virtual intercept of the large semicircle observed in the impedance plots. The resistance of the sample changes clearly with the different partial pressures of water and seems to reach equilibrium in a surprisingly short time. The bulk resistance did not change with time or partial pressure of water.

Figure 8 displays the logarithm of the total conductivity of the sample, with the grain boundary as the major component, as a function of the logarithm of the partial pressure of water. The dependence is very clear and the slope indicates a classic dependence according to Wagner's incorporation reaction:

$$H_2O + V_O^{\bullet\bullet} + O_O^x \rightarrow 2OH_O^{\bullet} \quad (2)$$

The reaction constant is

$$K = \frac{[OH_O^{\bullet}]^2}{p_{H_2O}[V_O^{\bullet\bullet}]} \quad (3)$$

and it can be assumed that at low partial pressure of water the oxygen vacancies are not saturated with hydroxyl

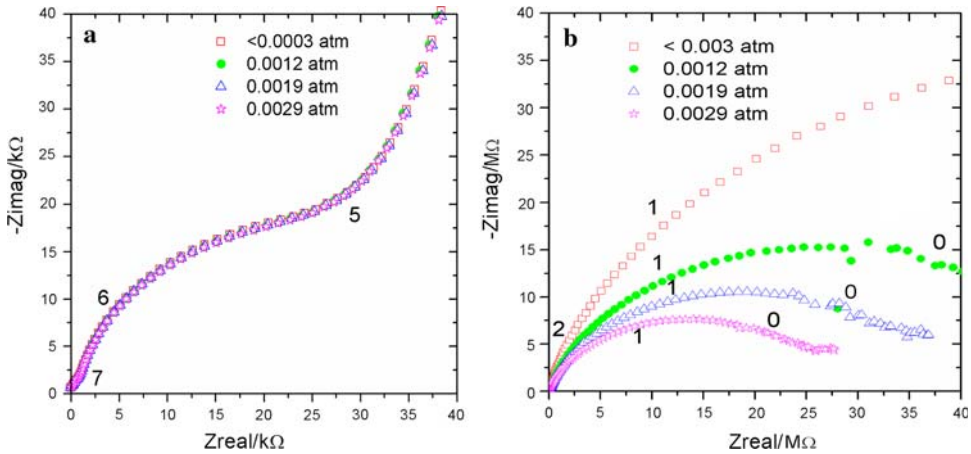


**Fig. 6** Impedance spectra of a sample measured in dry air and in wet air at 200 °C. Figure 6a displays the bulk response at high frequencies while Fig. 6b displays the whole spectra. The numbers indicate the logarithm of the frequency

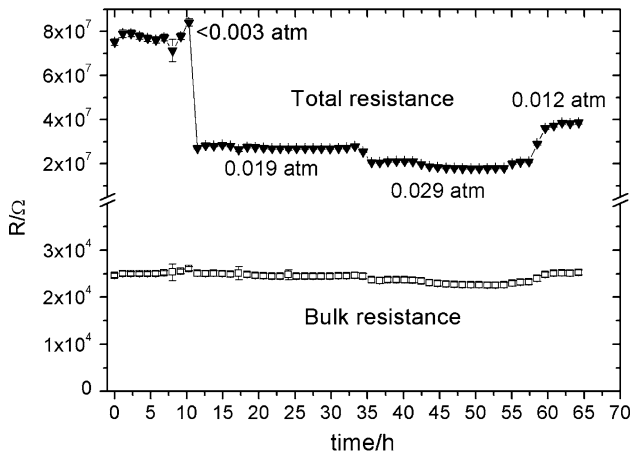


**Fig. 7** Total resistance and bulk resistance at 200 °C as a function of time for dry and wet air. The water partial pressures are indicated

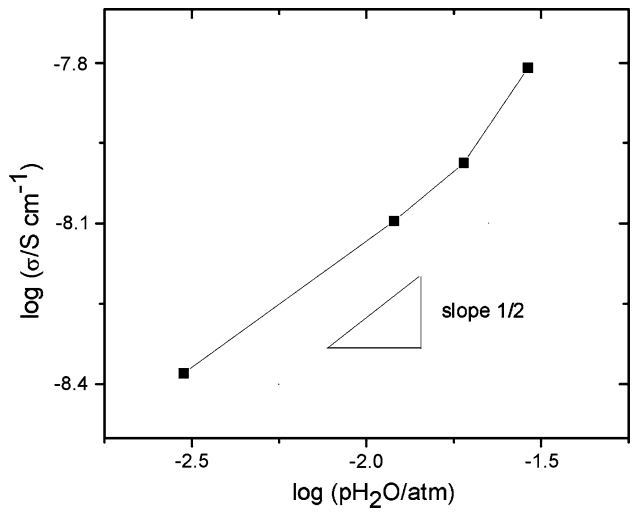


**Fig. 8** Logarithm of the conductivity as a function of log partial pressure of water

species and are at a constant level determined by the concentration of Gd dopant

$$[V_O^{\bullet\bullet}] \gg [OH_O^{\bullet}] \quad (4)$$

This leads to

$$p_{H_2O}^{1/2} \propto [OH_O^{\bullet}] \quad (5)$$

This is the general trend observed in Fig. 8. In view of the interesting results of Figs. 5, 6, 7, 8, it was assumed that the grain boundary transport has a protonic nature. These results are contrary to findings by Kim et al., who, whilst looking for the effect of water in the conductance of nanoceramics of this material, found no noticeable effect [23] whereas a change below 200 °C can be observed in this work, an interval not studied by them.

A discussion about possible paths for proton transport follows. Let us consider two possibilities: a) the observed conductivity is due to transport on a surface or b) the transport takes place in the grain boundaries.

a) Surface conductivity. It should be recalled than the samples were brittle and might have cracked during the measurements, although a simple inspection did not reveal any damage after the experiments. Nonetheless, the origin of such large resistances as observed in Fig. 6b in the wet atmospheres may be related to the presence of cracks. It is a known fact that the surface of cerium oxide is catalytically very active [24] and that a variety of molecules, including water, can be trapped in the surface of the nanoparticles [25]. Indeed the absorption of water into the pores of nanoceramics of Gd-doped ceria has been reported before [23]. It may well be that the absorption of water takes place on the surface of cracks, surfaces that, as a result of segregation, might contain an accumulation of $Gd_2O_3$ [26], a well known proton conductor [27]. The occurrence of surface conductivity might explain the fast equilibration time upon atmosphere change as seen in Fig. 7. Another point in favour of this idea is the small

activation energies seen in Fig. 5: 0.18 eV for wet and 0.26 eV for dry conditions These do not seem to reflect oxygen transport. On the other hand, the values are remarkably similar to those found by Raz et al. in the fluorite analogue YSZ [28]. They report an activation energy of 0.30 eV for proton transport in a chemisorbed water layer on the surface of YSZ. That activation energy consists of 0.19 eV for the migration plus half the enthalpy of formation of a defect, 0.11 eV.

b) Grain boundary conductivity. The capacitance values obtained for the large semicircles seen in Fig. 6b are around 76 nF, a typical value for a grain boundary and far too small for an electrode response. The segregation of the dopant to the grain boundaries of ceria reported in the literature may be taking place here therefore bringing about the incorporation of water into the nanoceramics [26]. The lanthanides sesquioxides such as $Gd_2O_3$ incorporate water into their lattice to produce proton conduction [27]. Furthermore, the recent reports of Kim et al. [7] seem to indicate the presence of proton conduction along grain boundaries but only in samples of grain size below 15 nm. In this work, this grain size average is considerably larger. Nonetheless, it should be recalled that they used spark plasma sintering, a preparation method that, due to its nature, might yield a very different grain boundary structure and/or composition.

A series of experiments to estimate the mobility of oxygen in the grain boundaries in these nanoceramics are currently being performed. Among future work, the Secondary Ion Mass Spectrometry technique will be of great help as one can obtain information on the diffusivity of oxygen and the concentration of protons as has been done for other materials in the past [29, 30].

## 4 Conclusions

Dense doped ceria samples with grain sizes from 91 nm to 252 nm were prepared. The large number of interfaces in the sample increases the total resistance, due to the large grain boundary component. The specific grain boundary activation energy of 1 eV clearly hints at the same type of grain boundary transport in these samples when measured in atmospheric air, but the order of magnitude did not show a clear trend with grain size. A sample sintered in a wet atmosphere showed a clear conductivity dependence with partial pressure of water, but it is not clear as yet if this is due to surface or grain boundary conductivity. According to the results shown, water does not seem to affect the bulk properties of Gd-doped $CeO_2$ in the temperature range measured. Figures 5, 6, 7, 8 confirm the influence of water on the electrical conductivity. This interesting result calls for more research into these nanoceramics as potential materials for electrochemical applications at very low temperatures.

**Acknowledgments** We thank D. Cummings for help with the automation of the measurements and M. Chan for help in the preparation of some samples. ERT thanks *Dirección General de Asuntos del Personal Académico—Universidad Nacional Autónoma de México* for a sabbatical grant.

## References

1. Ruiz-Trejo E, Sirman JD, Baikov Yu M et al (1998) Solid State Ionics 113:565
2. Huang KM, Feng M, Goodenough JB (1998) J Am Ceram Soc 81:357
3. Tuller HL, Nowick AS (1979) J Electrochem Soc 126:209
4. Yahiro H, Eguchi K, Arai H (1986) Solid State Ionics 21:37
5. Yokokawa H, Horita T, Sakai N et al (2004) Solid State Ionics 174:205
6. Yokokawa H, Horita T, Sakai N et al (2006) Solid State Ionics 177:1705
7. Kim S, Anselmi-Tamburini U, Park HJ et al (2008) Adv Mater 20:556
8. Chiang Y-M, Lavik EB, Kosacki I et al (1997) J Electroceram 1:7
9. Kim S, Maier J (2002) J Electrochem Soc 149:J73
10. Hwang JH, Mason TO (1998) Z Phys Chem 207:21
11. Tschöpe A, Sommer E, Birringer R (2001) Solid State Ionics 139:255
12. Bellino MG, Lamas DG, Walsöe de Reca NE (2006) Adv Funct Mater 16:107
13. Suzuki T, Kosacki I, Anderson HU (2002) Solid State Ionics 151:111
14. Jasinski P (2006) Solid State Ionics 177:2509
15. Ou DR, Mori T, Ye F et al (2006) Acta Mater 54:3737
16. Ruiz-Trejo E, Benítez-Rico A, Gómez-Reynoso S et al (2007) J Electrochem Soc 154:A258
17. Ruiz-Trejo E, Santoyo-Salazar J, Vilchis-Morales R et al (2007) J Solid State Chem 180:3093
18. Rupp J, Gauckler L (2006) Solid State Ionics 177:2513
19. Mendelson MI (1969) J Am Ceram Soc 52:443
20. Hsu CH, Mansfeld F (2001) Corrosion 57:747
21. Steele BCH (2000) Solid State Ionics 129:95
22. Christie GM, van Berkel FPF (1996) Solid State Ionics 83:17
23. Kim S, Merkle R, Maier J (2003) Solid State Ionics 161:113
24. Trovarelli A, de Leitenburg C, Boaro M et al (1999) Catal Today 50:353
25. Azki MI, Hasan MA, Al-Sagheer FA (2001) Coll Surf A 190:261
26. Scanlon PJ, Bink RAM, van Berkel FPF et al (1998) Solid State Ionics 112:123
27. Norby T, Dyrlie O, Kofstad P (1992) J Am Ceram Soc 75:1176
28. Raz S, Sasaki K, Maier J et al (2001) Solid State Ionics 143:181
29. Ruiz-Trejo E, Kilner JA (1997) Solid State Ionics 97:529
30. Ruiz-Trejo E, Kilner JA (2000) Solid State Ionics 130:313